Journal of Electronic Research and Application, 2026, Volume 10, Issue 3
http://ojs.bbwpublisher.com/index.php/JERA
ISSN Online: 2208-3510
ISSN Print: 2208-3502

Dynamics of Electric Field Perturbation in Gold Nanobipyramids During Dual-Pulse Two-Photon Coherent Excitation

Qiong Li, Yao Li*

Third Hospital of Shanxi Medical University, Shanxi Bethune Hospital, Shanxi Academy of Medical Sciences, Tongji Shanxi Hospital, Taiyuan, 030032, China

***Corresponding author:** *Yao Li, liyao@sxbqeh.com.cn*

Copyright: © 2026 Author(s). This is an open-access article distributed under the terms of the Creative Commons Attribution License (CC BY 4.0), permitting distribution and reproduction in any medium, provided the original work is cited.

Abstract: Optical-based microwave electric field detection has emerged as a research hotspot due to its advantages of high spatial resolution and immunity to electromagnetic interference. However, existing techniques are often limited by their sensitivity or reliance on specialized fluorescent materials. Gold nanobipyramids (AuNBPs), serving as nanoprobes with tip-enhancement effects and a well-defined three-level system, exhibit high sensitivity in their two-photon photoluminescence (TPPL) process to phase perturbations and plasmon resonance changes induced by microwave fields. By establishing a quantitative mapping model between microwave intensity and TPPL signal strength, we achieved an absolute measurement of microwave field strength with a spatial resolution that breaks the 100-nanometer barrier. Through comparative analysis of microwave responses under different pulse delays, we reveal that the microwave field primarily modulates TPPL intensity by interfering with the coherent excitation pathway. The most significant response of TPPL intensity to microwave power was observed near the zero-delay point, where the quantum coherence is strongest.

Keywords: Two-photon photoluminescence; Dual-pulse coherent excitation; Gold nanobipyramids; Microwave electric field perturbation

Online publication: April 22, 2026

1. Introduction

Microwave measurement technology, a cornerstone of the modern information society, plays an indispensable role in high-speed communications, precision radar, Earth observation, and remote sensing [1–3]. Traditional microwave detection primarily relies on electrical probes (e.g., dipole antennas, semiconductor probes) that measure field strength via electromagnetic induction. However, limited by device size and electromagnetic coupling effects, the spatial resolution of these methods is typically confined to the millimeter or even centimeter scale. This constraint makes precise mapping and visualization of field distributions at micro- and nano-scales extremely challenging,

severely hindering their application in frontier scenarios such as integrated circuit near-field analysis and biological electromagnetic effect monitoring [4].

To overcome these limitations, optically read microwave electric field sensing techniques have been developed. These methods leverage the nonlinear interaction between light and matter under a microwave field, converting microwave signals into optical responses for measurement. They offer combined advantages of non-invasiveness, high spatial resolution, and immunity to electromagnetic interference, making them an international research focus [5,6]. Existing optical approaches include polarization modulation based on electro-optic crystals, electromagnetically induced transparency based on Rydberg atoms, [2-4][2-4]and intensity detection based on fluorescent materials [7–9]. However, these methods face significant challenges: electro-optic crystals have limited sensitivity, atomic systems require complex vacuum environments, and fluorescent probes are prone to photobleaching and rely on external labeling, complicating their use in complex *in-situ* systems [10,11]. Therefore, there is a pressing need to develop a novel optical mechanism for microwave field detection that combines high sensitivity, nano-scale spatial resolution, and label-free operation.

To overcome these limitations, optically read microwave electric field sensing techniques have been developed. These methods leverage the nonlinear interaction between light and matter under a microwave field, converting microwave signals into optical responses for measurement. They offer combined advantages of non-invasiveness, high spatial resolution, and immunity to electromagnetic interference, making them an international research focus [5,6]. Existing optical approaches include polarization modulation based on electro-optic crystals, electromagnetically induced transparency based on Rydberg atoms, and intensity detection based on fluorescent materials [7–9]. However, these methods face significant challenges: electro-optic crystals have limited sensitivity, atomic systems require complex vacuum environments, and fluorescent probes are prone to photobleaching and rely on external labeling, complicating their use in complex in-situ systems [10,11]. Therefore, there is a pressing need to develop a novel optical mechanism for microwave field detection that combines high sensitivity, nano-scale spatial resolution, and label-free operation.

2. Results and discussion

The presence of an intermediate state in the TPPL process of AuNBPs grants them excellent phase sensitivity and nonlinear coherent enhancement effects under dual-pulse coherent excitation, as systematically studied in our prior work [16,17]. The model is illustrated in **Figure 1b**. Experimentally, as shown in **Figure 1a**, Pulse 1 and Pulse 2, with controlled delay and phase characteristics, excite the AuNBPs. The microwave signal is emitted from an antenna connected to a microwave source, directed at the sample stage, with microwave-absorbing foam placed around to prevent reflections that could alter microwave power.

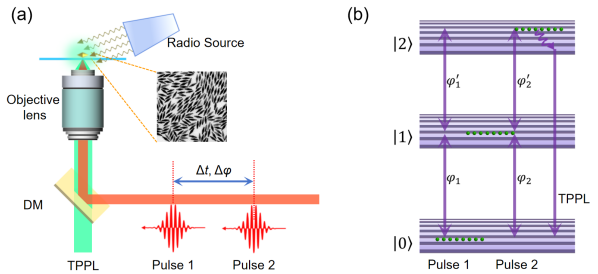

Figure 1. Schematic of the experimental setup and the DP-TPPL model for AuNBPs. (a) Experimental setup. Pulses with controlled delay and phase excite AuNBPs; the TPPL signal is collected by an objective lens, filtered, and detected. DM: Dichroic Mirror. (b) Coherent excitation DP-TPPL model for AuNBPs, illustrating the real intermediate state and the coherence-dominated TPPL process. F1 and F2 represent the electric field vectors of the two pulses.

We first verified that the microwave-affected photoluminescence from AuNBPs originates primarily from TPPL, not second-harmonic generation (SHG). As shown in **Figure 2**, we compared the photoluminescence spectra of AuNBPs excited by femtosecond lasers with different bandwidths: 800 nm, 15 fs (80 nm bandwidth) and 1040 nm, 80 fs (10 nm bandwidth). Under 800 nm excitation at a very low pulse energy (< 0.625 pJ), the signal is dominated by TPPL (**Figure 2a**). In contrast, 1040 nm excitation at a much higher pulse energy (100 pJ) produces a prominent SHG signal (**Figure 2b**). For symmetric AuNBPs, the narrow-band 1040 nm laser requires high energy, potentially causing deformation and breaking symmetry to generate SHG. The broadband 800 nm laser provides efficient TPPL for microwave detection at ultralow pulse energies without damaging the particles.

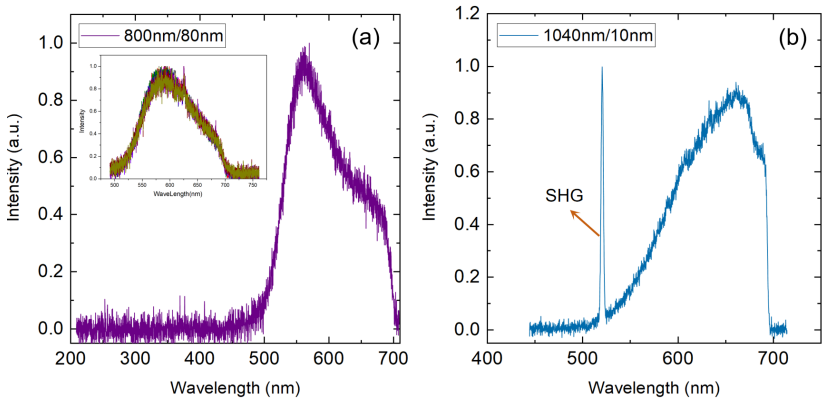

Figure 2. TPPL versus SHG in AuNBPs. (a) Spectrum under 800 nm, 15 fs excitation (0.625 pJ). (b) Spectrum under 1040 nm, 80 fs excitation (100 pJ).

Given their coherent response, we tested the microwave response of AuNBPs. **Figure 3** shows that the TPPL signal from AuNBPs (70 nm long axis, 20 nm short axis) responds mainly around 2.0 GHz at a fixed microwave power of 10 dBm.

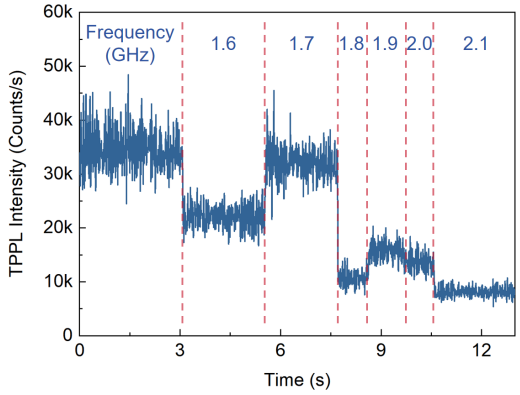

Figure 3. Response of AuNBPs TPPL to microwave radiation at different frequencies (microwave power: 10 dBm).

A continuous frequency scan from 1.98 GHz to 2.06 GHz (**Figure 4a**) shows that the microwave field attenuates the TPPL signal. Analysis of the intensity change ΔI (**Figure 4b**) reveals a characteristic peak that can fit with a Gaussian lineshape (orange-red line), suggesting a direct relationship between the microwave response and electron population.

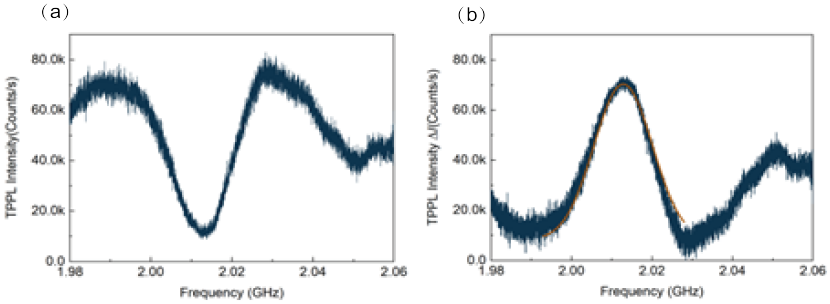

Figure 4. Response of AuNBPs TPPL to microwave frequencies in the 1.98-2.06 GHz range. (a) TPPL intensity vs. frequency. (b) TPPL intensity change ΔI vs. frequency with Gaussian fit.

2.1. Mechanism of microwave response

The 2 GHz microwave photons possess negligible energy and cannot directly induce electronic transitions. However, the oscillating electric field can perturb the relaxing non-equilibrium electron distribution created by the femtosecond laser, altering the electron energy distribution or population, which in turn affects the radiative recombination rate and modulates the luminescence intensity. Theoretically, after femtosecond excitation, the electron system can be described by a Fermi-Dirac distribution with an elevated electron temperature T_e:

$$f_e(E,t=0^+)\approx[1+exp((E-E_F)/(k_BT_e))]^{-1} \quad (1)$$

Where T_e is on the order of hundreds of Kelvins and cools on a picosecond scale via electron-phonon scattering.

The microwave field $E_{mw}(t)=E_0cos(\omega_{mw}t)$ acts as a driving source, performing work on the electrons and continuously perturbing their distribution. Within the relaxation time approximation, this process is understood via a linearized Boltzmann equation:

$$\partial\delta f/\partial t = -\delta f/\tau - eE_{\mathrm{mw}}(t)\cdot v\,(\partial f_0/\partial E) \quad (2)$$

Where τ is the electron momentum relaxation time (~10-30 fs for gold).

This perturbation directly alters the hot electron population. The PL intensity $I_{\mathrm{PL}}(t)$ is proportional to the product of the hot electron population $n_{hot}(t)$ and the radiative recombination rate $\Gamma_{ra}d$:

$$I_{\mathrm{PL}}(t)\propto\Gamma_{\mathrm{rad}}\cdot\int_{E_F+\hbar\omega_{\mathrm{PL}}}^{\infty}D\,(E)\cdot f_e(E,t)dE \quad (3)$$

The microwave-induced perturbation δf to the distribution function thus directly modulates $I_{\mathrm{PL}}(t)$. Under weak-field, low-frequency ($\omega_{\mathrm{mw}}\tau\ll 1$) conditions, the relative modulation depth can be estimated as $\Delta I_{\mathrm{PL}}/I_{\mathrm{PL0}}\propto(|eE_0|^2\tau^2)/(m^*k_BT_e)\cdot\tau_{\mathrm{eff}}/[1+(\omega_{\mathrm{mw}}\tau_{\mathrm{eff}})^2]$. This indicates that the modulation depth is proportional to the microwave power ($\propto|E_0|^2$) and is tightly linked to the characteristic temperature T_e and effective lifetime τ_{eff} (~hundreds of fs to ps) of the non-equilibrium electrons, explaining why this modulation is observable only within the short temporal window following femtosecond laser excitation.

Based on this, we investigated the microwave power-dependent response. As shown in **Figure 5**, the TPPL intensity of AuNBPs decreases gradually with increasing microwave power, following a Boltzmann function fit with $R^2 > 0.99$.

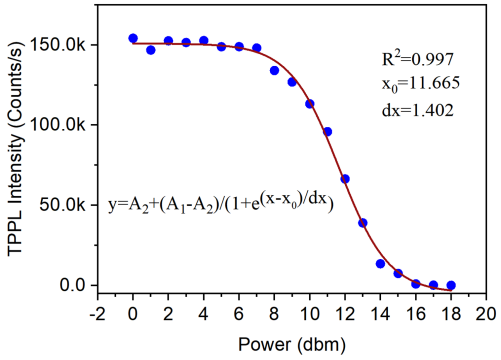

Figure 5. Power-dependent response of AuNBPs TPPL to 2.0 GHz microwave radiation. Blue dots: experimental data; red line: Boltzmann function fit. Key fitting parameters x_0 and dx are indicated.

In **Figure 5**, A2 and A1 define the response range of the TPPL intensity. The parameters x_0 and dx are the half-activation power and slope factor, respectively. Here, x_0 = 11.665 dBm, corresponding to an electric field strength of approximately 0.849 V/m, which is lower than typical biological field strengths. A slope factor dx > 1 demonstrates the high sensitivity of AuNBPs for microwave measurement. The successful Boltzmann fit further suggests that the microwave perturbation directly affects the electron population in the three-level system during the TPPL process [18]. Our prior work confirmed that the DP-TPPL in AuNBPs, due to the intermediate state, shows a sensitive phase response, allowing TPPL enhancement by two orders of magnitude via phase control [17]. Therefore, we studied the effect of microwave fields on TPPL intensity under different dual-pulse delays.

Green arrows in **Figure 6** indicate the TPPL intensity with and without the microwave field at different delays. Comparison shows that while single-pulse excitation involves the intermediate state, the microwave influence time is limited (~15 fs pulse width), resulting in a small ratio a1:a2 = 1.14. At longer delays (b, $\Delta t \approx 83$ fs), within the intermediate state lifetime, the microwave effect increases, yielding b1:b2 = 1.79. When the pulse interval is further reduced to near zero delay (c), the microwave interaction time relative to case (b) is shorter, yet the largest ratio c1:c2 = 1.90 is observed. This is because at zero delay, AuNBPs exhibit the strongest quantum coherence under dual-pulse excitation, and this intermediate-state-dominated coherence is more susceptible to microwave disruption, leading to a greater reduction in DP-TPPL [19].

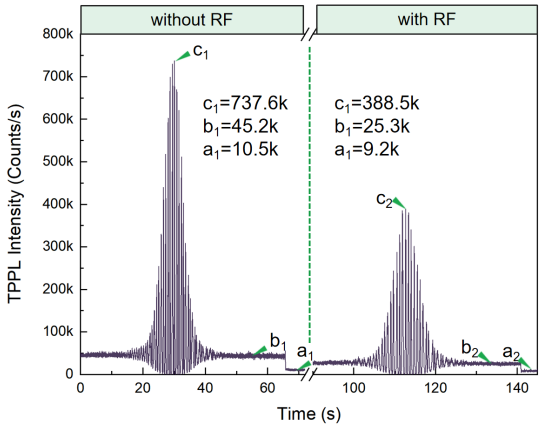

Figure 6. Response of AuNBPs TPPL to 2.0 GHz microwave radiation at different time delays. a1 (a2): TPPL intensity under single-pulse excitation without (with) microwave field (RF). b1, c1 (b2, c2): DP-TPPL intensity at delays $\Delta t \approx 83$ fs and $\Delta t \approx 0$ without (with) microwave field, respectively.

3. Conclusion

This study developed a microwave electric field measurement method based on the dual-pulse two-photon photoluminescence of gold nanobipyramids. Experimental results demonstrate that this method leverages the plasmonic properties and three-level system of AuNBPs, enabling the detection of microwave fields via dual-pulse femtosecond laser excitation. AuNBPs with dimensions of 70 nm × 20 nm showed a selective response to a 2.0 GHz microwave frequency. The microwave electric field alters their plasmon resonance characteristics, thereby affecting TPPL intensity. A quantitative relationship between microwave field strength and TPPL signal was established via Boltzmann function fitting. Effective detection was achieved using 800 nm, 15-fs femtosecond laser pulses at single-pulse energies below 0.625 pJ, with a spatial resolution that reached the sub-100-nanometer level. Compared to conventional methods, this approach is label-free and robust against interference. Experiments with different pulse delays indicate that the microwave field primarily modulates the TPPL signal by affecting intermediate-state population and the coherent excitation process, with the most significant response observed near zero time delay. This work presents a novel detection tool for analyzing electromagnetic fields at micro- and nanoscales.

Funding

National Natural Science Foundation of China (Project No.: 62205190); China Postdoctoral Science Foundation (Project No.: 2022M722003 and 2024T170536); Shanxi Basic Research Program (Project No.: 202203021212100); Shanxi Bethune Hospital Scientific Research Startup Fund (Project No.: 2021RC032); Central Guiding Local Science and Technology Development Fund Project (Project No.: YDZJSX2025D072).

Disclosure statement

The authors declare no conflict of interest.

References

[1] Zou X, Lu B, Pan W, et al., 2016, Photonics for Microwave Measurements. Laser & Photonics Reviews, 10(5): 711.

[2] Hempel H, Savenjie T, Stolterfoht M, et al., 2022, Predicting Solar Cell Performance from Terahertz and Microwave Spectroscopy. Advanced Energy Materials, 12(13): 2102776.

[3] Réouven A, Rémy D, Théau P, et al., 2023, Quantum Advantage in Microwave Quantum Radar. Nature Physics, 19(10): 1418.

[4] Wright E, 1999, MAP: the Microwave Anisotropy Probe. New Astronomy Reviews, 43(2–4) 257.

[5] Zou X, Lu B, Pan W, et al., 2016, Photonics for Microwave Measurements. Laser & Photonics Reviews, 10(5): 700.

[6] Janusz M, Amjed H, Andrew M, et al., 2024, Ultra-Wideband RF-Photonics Technology for Microwave Spectrometry. IEEE Journal of Selected Topics in Applied Earth Observations and Remote Sensing, 2024: 1716100.

[7] Yang C, Yu Y, Li J, et al., 2022, Sequential Generation of Multiphoton Entanglement with a Rydberg Superatom. Nature Photonics, 16(9): 658.

[8] Andrea M, Léa L, Angelo C, et al., 2022, Optical Coherent Manipulation of Alkaline-Earth Circular Rydberg States. Nature Physics, 18(5): 502.

[9] Liu Z, Zhang L, Liu B, et al., 2022, Deep Learning Enhanced Rydberg Multifrequency Microwave Recognition.

Nature Communications, 13(1): 1997.

[10] Kwon J, Elgawish M, Shim S, 2022, Bleaching-Resistant Super-Resolution Fluorescence Microscopy. Advanced Science, 9(9): 2101817.

[11] Wang H, Han G, Tang H, et al., 2023, Synchronous Photoactivation-Imaging Fluorophores Break Limitations of Photobleaching and Phototoxicity in Live-Cell Microscopy. Analytical Chemistry, 95(44): 16243.

[12] Zhang P, Cai T, Zhou Q, et al., 2022, Ultrahigh Modulation Enhancement in All-Optical Si-based THz Modulators Integrated with Gold Nanobipyramids. Nano Letters, 22(4): 1541.

[13] Huang J, Jiang F, Zhao Z, et al., 2024, Gold Nanobipyramid-based Photothermal Sensors for the Portable Evaluation of Total Antioxidant Capacity. ACS Applied Nano Materials, 7(12): 14621.

[14] Yu Y, Li Y, Qin H, et al., 2020, Microwave Measurement and Imaging for Multiple Corrosion Cracks in Planar Metals. Materials & Design, 202: 196109151.

[15] Tao Y, Yang F, Tao Z, et al., 2022, Fully On-Chip Microwave Photonic Instantaneous Frequency Measurement System. Laser & Photonics Reviews, 16(11): 2200158.

[16] Li Y, Qin C, Song Y, et al., 2021, Great Enhancement on Two-Photon Photoluminescence Imaging Contrast of Au Nanoparticles via Double-Pulse Femtosecond Laser Excitation with Controlled Phase Differences. Optics Express, 29(15): 22855.

[17] Li Y, Yang Y, Qin C, et al., 2021, Coherent Interference Fringes of Two-Photon Photoluminescence in Individual Au Nanoparticles: The Critical Role of the Intermediate State. Physical Review Letters, 127(7): 073902.

[18] van Swieten T, Merlijn S, Auke V, et al., 2022, Extending the Dynamic Temperature Range of Boltzmann Thermometers. Light: Science & Applications, 11(1).

Publisher's note

Bio-Byword Scientific Publishing remains neutral with regard to jurisdictional claims in published maps and institutional affiliations.